



# Intestinal epithelial $\beta$ Klotho is a critical protective factor in alcohol-induced intestinal barrier dysfunction and liver injury

Zhengping Hou,<sup>a,1</sup> Qiuying Ding,<sup>a,1</sup> Yuqi Li,<sup>a,1</sup> Zhibo Zhao,<sup>a</sup> Fang Yan,<sup>d</sup> Yanping Li,<sup>a</sup> Xingxing Wang,<sup>a</sup> Jingyuan Xu,<sup>a</sup> Weiting Chen,<sup>a</sup> Guicheng Wu,<sup>c,2</sup> Xiongzong Ruan,<sup>a,b,2</sup> and Lei Zhao<sup>a,2\*</sup>

<sup>a</sup>Centre for Lipid Research, Key Laboratory of Molecular Biology for Infectious Diseases, Ministry of Education, The Second Affiliated Hospital, Chongqing Medical University, Chongqing 400016, China

<sup>b</sup>John Moorhead Research Laboratory, Centre for Nephrology, University College London Medical School, Royal Free Campus, University College London, London NW3 2PF, United Kingdom

<sup>c</sup>Department of Hepatology, Chongqing University Three Gorges Hospital, School of Medicine, Chongqing University, Chongqing 404000, China

<sup>d</sup>Center for Medicine Research and Translation, The Affiliated Fifth People's Hospital of Chengdu University of Traditional Chinese Medicine, Chengdu 610000, China

## Summary

**Background** Intestinal barrier dysfunction is crucial in alcohol-associated liver disease (ALD). The decreased beta-Klotho (KLB) expression caused by gene variation is associated with hyperpermeability in patients with irritable bowel syndrome. Here we investigated the roles of intestinal KLB in maintaining the intestinal epithelial barrier in ALD and the underlying mechanisms.

**Methods** We constructed the intestine-specific overexpression KLB mice to investigate the role of KLB on alcohol-induced intestinal barrier dysfunction and liver injury in an ALD mouse model. To investigate the molecular mechanism *in vitro*, Caco2 cells were cultured and infected with the KLB overexpression lentivirus, or transfected with KLB/TRPV6 siRNA, or TRPV6/FXR1 overexpression plasmid, and treated with or without ethanol.

**Findings** The upregulation of KLB in enterocytes effectively protected mice from alcohol-induced intestinal barrier hyperpermeability, thereby ameliorating hepatic steatosis and inflammation. KLB competitively suppressed FXR1 binding to the TRPV6 mRNA, increasing TRPV6 mRNA stability and protein abundance in intestinal epithelial cells. Furthermore, KLB formed a complex with TRPV6 and tight junction (TJ) proteins, protecting against alcohol-induced TJ proteins endocytosis and degradation as well as intestinal barrier impairment.

**Interpretation** This work suggested that KLB attenuated alcohol-induced intestinal epithelial barrier dysfunction and liver injury through FXR1/TRPV6/TJ proteins pathway.

**Funding** National Natural Science Foundation of China, Chongqing Natural Science Foundation, Talent Project of Chongqing and the Science and Technology Research Program of Chongqing Municipal Education Commission.

**Copyright** © 2022 The Authors. Published by Elsevier B.V. This is an open access article under the CC BY-NC-ND license (<http://creativecommons.org/licenses/by-nc-nd/4.0/>)

**Keywords:** Beta-Klotho; Intestinal barrier dysfunction; Transient receptor potential vanilloid subtype 6; Fragile X mental retardation syndrome-related protein 1

## Introduction

Alcohol-associated liver disease (ALD) is a major cause of chronic liver disease worldwide. ALD comprises a

range of liver disorders related to alcohol abuse, including alcoholic fatty liver (simple steatosis), alcoholic steatohepatitis, cirrhosis, and liver cancer in the end-stage.<sup>1</sup> As the World Health Organization (WHO) currently estimates, three million people die annually from alcohol-associated diseases.<sup>2</sup> Although significant progress has been made in our understanding of the pathological process of ALD, the mechanisms of ALD remain unclear and effective treatment options for ALD are limited.

\*Corresponding author.

E-mail address: zhaolei@cqmu.edu.cn (L. Zhao).

<sup>1</sup> These authors contribute equally.

<sup>2</sup> These authors share similar correspondence authorship.

### Research in context

#### *Evidence before this study*

Alcohol-associated liver disease (ALD) is a major cause of chronic liver disease worldwide. Recent reports demonstrate that intestinal barrier dysfunction plays a critical role in alcohol-induced liver injury. Beta-Klotho (KLB) is a single-pass transmembrane protein, which is widely expressed in multiple tissues, such as adipose tissue, pancreas and gut. The decreased KLB expression caused by gene variation is associated with increased intestinal permeability in patients with irritable bowel syndrome with diarrhea. However, the role of KLB in intestinal barrier and ALD remains unclear.

#### *Added value of this study*

In present study, we reported that alcohol reduced intestinal epithelial KLB expression in an ALD mouse model via inhibiting transcriptional factor HNF4A, while the upregulation of KLB in enterocytes effectively protected mice from alcohol-induced intestinal barrier hyperpermeability, thereby ameliorating ALD. Mechanically, KLB increased transient receptor potential vanilloid subtype 6 (TRPV6) mRNA stability and protein abundance by competitively suppressing fragile X mental retardation syndrome-related protein 1 (FXR1) binding to the TRPV6 mRNA in intestinal epithelial cells. Furthermore, KLB formed a complex with TRPV6 and tight junction (TJ) proteins (ZO-1 and Occludin), protecting against alcohol-induced tight junction proteins endocytosis and degradation as well as intestinal barrier impairment.

#### *Implications of all the available evidence*

We provide fine evidence supporting that intestinal epithelial KLB is a critical protective factor in alcohol-induced intestinal barrier dysfunction and subsequent liver injury. Our data suggest activating intestinal KLB may be a new strategy for preventing alcohol-induced intestinal barrier impairment and liver injury as well as other intestinal barrier dysfunction-associated diseases.

In recent years, the importance of the gut-liver axis in ALD pathogenesis has been well recognized. Extensive evidence from ALD patients and animal models with ALD has demonstrated that alcohol consumption induces intestinal epithelial barrier impairment and gut microflora dysbiosis.<sup>3</sup> Indeed, the intestinal epithelium fundamentally acts as a physical barrier between luminal contents, such as the intestinal microbiota, the underlying mucosal immune system, and the remainder of the food.<sup>4</sup> When the intestinal epithelial barrier is impaired, numerous microorganisms and microbial products, such as the gram-negative bacteria cell wall component lipopolysaccharide (LPS), enter into the liver through the portal vein as microbiota-associated molecular patterns (MAMPs). MAMPs recruit and activate

Kupffer cells and lymphocytes to induce hepatic steatosis, inflammation, and fibrosis, causing the development and progression of ALD, even carcinogenesis.<sup>5</sup> Previous studies have suggested that ameliorating gut microbiota dysbiosis may alleviate alcohol-induced hepatic steatosis, inflammation, and fibrosis.<sup>6</sup> However, the regulatory mechanism(s) underlying intestinal epithelial barrier function in ALD is not fully understood.

As a member of klotho gene family proteins,  $\beta$  Klotho (KLB) is a single-pass transmembrane protein, which is widely expressed in multiple tissues, such as adipose tissue, pancreas and gut.<sup>7</sup> In adipose tissue and neurons, KLB acts as a co-receptor of fibroblast growth factor receptor (FGFR), mediating fibroblast growth factor 21 (FGF21) and fibroblast growth factor 15/19, to regulate glucose and lipid metabolism.<sup>8,9</sup> It also regulates bile acids (BA) synthesis and excretion in the liver.<sup>10</sup> Several KLB single-nucleotide polymorphisms (SNPs) have been linked to obesity and hepatic inflammation, suggesting that they may play a role in metabolic associated fatty liver disease (MAFLD).<sup>11</sup> One of the SNPs, rs17618244, which has the potential to lower KLB expression via affecting KLB protein stability,<sup>12</sup> is linked to hepatic ballooning and fibrosis, inflammation, and cirrhosis in both pediatric and obese MAFLD patients.<sup>13,14</sup> In addition, genome-wide association studies (GWAS) data have shown that KLB SNPs (rs1190694, rs9991733 and rs13130794) were associated with alcohol consumption in human.<sup>15,16</sup> Brain KLB knockout mice exhibit an increase in alcohol preference.<sup>17</sup> In the gut, the decreased KLB expression caused by gene variation is associated with increased intestinal permeability in patients with irritable bowel syndrome with diarrhea,<sup>12</sup> suggesting that the downregulated KLB may play a role in alcohol-induced intestinal epithelial dysfunction and liver injury.

From apical-to-basal, the paracellular space between intestinal epithelial cells is sealed with tight junction (TJ), zonula occludens), adherens junction (zonula adherens), and desmosomes.<sup>18</sup> TJ is the primary determinant of paracellular permeability, which is essential for maintaining intestinal epithelial barrier function.<sup>19</sup> As the first identified TJ protein, Occludin, is a ~65kDa transmembrane protein with two flexible extracellular loops constructing a zipper-like structure to interdigitate with adjacent cells.<sup>20</sup> ZO-1 is a multidomain scaffolding protein, the N-terminal region of which interacts with Occludin and stabilizes the assembly of TJ.<sup>21</sup> It has been demonstrated that alcohol exposure reduces ZO-1 and Occludin expression in the intestinal epithelium with unclear mechanisms.<sup>22,23</sup>

Transient receptor potential vanilloid subtype 6 (TRPV6) is a crucial  $\text{Ca}^{2+}$  selective ion channel in intestinal epithelial tissues.<sup>24</sup> Besides its 6-transmembrane segment spanning ion channels, TRPV6 possess a C-terminal TRP domain and an N-terminal domain with six ankyrin repeats implicated in protein-protein

interactions.<sup>25</sup> Indeed, Kärki et al. found that TRPV6 was colocalized with E-cadherin, and TRPV6 knock-down not only reduced intracellular Ca<sup>2+</sup> levels but also disrupted junctional integrity in mammary epithelial cells.<sup>26</sup> Previous reports found that Klotho, which shares high levels of similarity with KLB, stimulates cell surface abundance and activity of TRPV5 in kidney cells.<sup>27,28</sup> Thus, we hypothesized that intestinal KLB might modulate TJ proteins expression and distribution via TRPV6, involved in alcohol-induced intestinal barrier impairment and ALD.

In the present study, we showed that alcohol reduced intestinal epithelial KLB expression in the ALD mouse model via inhibiting hepatocyte nuclear factor 4-alpha (HNF4A). The upregulation of KLB in enterocytes effectively protected mice from alcohol-induced intestinal villus damage and barrier hyperpermeability, thereby ameliorating hepatic steatosis and inflammation. We further demonstrated that KLB promoted the mRNA stability of TRPV6 and the formation of KLB/TRPV6/Occludin/ZO-1 complex is essential for maintaining intestinal barrier. Our data suggest activating intestinal KLB might be a new strategy for preventing alcohol-induced intestinal barrier impairment and liver injury.

## Materials and methods

### Ethics statement

The Institutional Animal Care and Use Committee of Chongqing Medical University (CQMU) and Chongqing University Three Gorges Hospital approved all experimental procedures and protocols used in this study (Approval NO. 2019004, NO. 2020-10).

### Animal models

Thirty-five mice were included in this study, and all animal procedures were performed in accordance with the Guide for Care and Use of Laboratory Animals of CQMU and Chongqing University Three Gorges Hospital. C57BL/6 female mice (8-10 weeks of age) were provided by Chongqing Medical University (Chongqing, CHN). For the establishment of ALD model in C57BL/6 mice,<sup>29-31</sup> ten female mice (average body weight, 16-18 g) were randomly assigned to alcohol-fed (AF) group ( $n=5$ ) or pair-fed (PF) group ( $n=5$ ). The AF group mice were fed a 5% (w/v) alcohol-containing Lieber-DeCarli liquid diet (Trophic cat#TP4231, Nantong, CHN) and the PF group mice received the isocaloric control liquid diet containing maltose dextrin in place of ethanol for 4 weeks. Based on the FLEX-ON system,<sup>32</sup> the intestine-specific KLB overexpression mice and negative control mice were generated by administering PVillin-Cre (C57BL/6 strain) female mice (Cyagen, CA, USA) with AAV9-FLEX-KLB-3Flag (AAV-KLB) purchased from GeneChem (Shanghai, CHN) or AAV9-FLEX-negative control-3Flag (AAV-NC) at a dose of

10<sup>11</sup> viral particles per 200  $\mu$ l per mouse via the tail vein. Twenty PVillin-Cre female mice (8-10 weeks of age, 16-18g of body weight) were randomly assigned to four groups (AAV-NC-PF, AAV-KLB-PF, AAV-NC-AF, AAV-KLB-AF,  $n=5$  in each group). Two weeks after AAV injection, these mice were fed with Lieber-DeCarli liquid diet with or without alcohol (5%, w/v). The PVillin-Cre female mice received injection of equal volume phosphate buffered saline were used as blank control ( $n=5$ ). The mice were kept in a pathogen-free, temperature-controlled environment with a 12-hour light/12 h dark cycle. After being anesthetized, blood samples and tissue samples were collected from mice.

### Serum assay and tissue lipid

Serum alanine aminotransferase (ALT) and aspartate aminotransferase (AST) were analyzed by an automatic biochemistry analyzer (HITACHI, Tokyo, JPN). For biochemical measurement of hepatic Triglyceride (TG) and total cholesterol (TC) content, liver tissues were collected from the same location of the livers and were prepared with the same weight. After the lipid was extracted from homogenized tissue, the lipid content was detected using commercial kits (Jiancheng Bioengineering Institute cat#A110-I-I, A111-I-I, Nanjing, CHN).

### Histological analysis

The liver and intestine tissues were embedded in paraffin and were cut into 5-micron-thick sections for Hematoxylin-Eosin (H&E, Beyotime cat#C0105S, Beijing, CHN) staining. Intestinal goblet cells were evaluated by Alcian Blue-Periodic Acid Schiff's staining (AB-PAS, Solarbio cat#G1285, Beijing, CHN). Frozen liver sections were stained with Oil Red O (ORO) (Solarbio cat#G1262) to visualize lipid droplets. Representative images of each study were obtained from six different fields in each sample.

### Endotoxin assay

For the measurement of serum endotoxin, the portal blood samples were collected in the endotoxin- and pyrogen-free test tubes from the mice following euthanasia. All operations were performed according to the reagent instructions of the Porteelite<sup>TM</sup> Rapid Fluorimetric Endotoxin Detection Kit (Lonza, BS, CHE). The absorbance at 540nm was determined by a microplate reader, and the LPS concentration was calculated according to the standard curve.

### Cell culture and treatments

Caco2 cells (RRID: CVCL\_0025) were purchased from ATCC (Manassas, VA, USA) and cultured in Dulbecco's Modification of Eagle's Medium (DMEM, Thermo Scientific cat#11965092, MA, USA), supplemented with 10% fetal bovine serum (FBS, Lonsera, UY) and 50 U/ml Penicillin-G, 50  $\mu$ g Streptomycin (Thermo Scientific cat#15140122). All cells tested negative for

mycoplasma, verified regularly using the Myco-Lumi Mycoplasma Detection Kit (Beyotime, Beijing, CHN, cat# C0297S). The cell identification report has been provided in the supplemental data. KLB-overexpressing lentiviruses were purchased from GeneChem (Shanghai, CHN) and small interfering RNA (siRNA) against KLB or TRPV6, FXR1 and TRPV6 overexpression vectors were purchased from GenePharma (Shanghai, CHN). To establish KLB overexpression (KLBOE) cells, Caco2 cells were infected with KLB-overexpressing lentivirus vectors and then selected with puromycin (Sangon cat#A606719, Beijing, CHN). The knockdown of KLB was achieved by transfecting the siRNA against KLB using Lipofectamine RNAi MAX (Invitrogen, USA). Inhibition or overexpression of TRPV6 and FXR1 were achieved by transfecting the appropriate siRNA mixed with Lipofectamine RNAi MAX (Invitrogen, USA) or appropriate plasmids mixed with ViaFect™-transfection reagent (Promega USA). Unless otherwise indicated, the transfected cells underwent further treatments 24 h after transfection and were harvested 48 hours after transfection.

For alcohol treatment, unless otherwise indicated, cells were cultured with DMEM medium containing 5% (v/v) alcohol (858.5 mM) for 24h to simulate *in vitro* intestinal barrier damage. For HNF4A-specific agonist treatment, Benfluorex (MedChemExpress cat#HY-B1058A, Shanghai, CHN) was added at a final concentration of 2  $\mu$ M in each well and incubated for two hours at 37°C. After selection, MG-132 (MedChemExpress cat#HY-13259) was used at 2  $\mu$ g/ml for 24 h and Dynasore (MedChemExpress cat#HY-15304) was used at 50  $\mu$ M for 30 min.

#### Immunofluorescence staining

Cells or frozen tissue sections were fixed with 4% paraformaldehyde for 10 min at room temperature and then incubated with 0.3% Triton-X 100 for 3 min, followed by blocking in phosphate-buffered saline (PBS, Sangon, Shanghai, CHN) containing 3% bovine serum albumin (BSA, Sangon) for 1 h. The primary antibodies were diluted at the appropriate dilutions and incubated with positive control samples and samples to be tested overnight at 4°C. For negative controls, samples were incubated with PBS overnight at 4°C. Then cells or sections were washed three times in PBS and incubated with fluorescence-conjugated secondary antibodies for 1 h at room temperature. Nuclei were stained with DAPI (Biosharp, Hefei, CHN) and the sections or cells were blocked with Antifade Mounting Medium (Beyotime, Beijing, CHN). Primary antibodies used were: F4/80 (Abcam cat#ab6640, MA, USA, RRID: AB\_1140040, dilution ratio 1:50), *Escherichia coli* (*E. coli*, Abcam cat#ab137967, RRID: AB\_2917966, dilution ratio:100), MUC2 (Proteintech cat#27675-1-AP, Wuhan, CHN, RRID: AB\_2880943, dilution ratio:100), Occludin (Proteintech cat#27260-1-AP,

RRID: AB\_2880820, dilution ratio:100), ZO-1 (Proteintech cat#21773-1-AP, RRID: AB\_10733242, dilution ratio:100), TRPV6 (Proteintech cat#13411-1-AP, RRID: AB\_2272390, dilution ratio:100), Flag (DYKDDDDK Tag) (Cell Signaling Technology cat#14793, Danvers, USA, RRID:AB\_2572291 dilution ratio:100), KLB (Aviva Systems cat#ARP53325\_P050, Santiago, USA, RRID: AB\_10640493, dilution ratio:100), Rab5 (Santa Cruz cat#sc-46692, CA, USA, RRID:AB\_628191, dilution ratio:100). Fluorescent secondary antibodies were goat anti-mouse fluorescein isothiocyanate (FITC)/Tetramethylrhodamine isothiocyanate (TRITC), goat anti-rabbit FITC/TRITC and goat anti-rat FITC/TRITC (ZSGB-BIO, Beijing, CHN dilution ratio:100). The antibody validation was provided in the supplemental data.

Fluorescent Images of samples were captured using laser confocal scanning microscopy (Leica). The relative fluorescence intensity (RFI) quantitation of images was performed using Images J (version 1.8.0) and Excel software, as previously described.<sup>33</sup> Firstly, the region of interest (ROI) was automatically selected using the “threshold” method. The mean fluorescence intensity (MFI) of target proteins on positive samples and negative controls was then measured. Finally, we used excel to calculate the final RFI using the following formula: Final RFI = MFI of ROI in images of positive samples – MFI of ROI in images of negative controls.

#### Intestine permeability measurement

Mice were fasted overnight and administered fluorescein isothiocyanate (FITC)-dextran 4000MW (FD4, Kaixin, Xi'an, CHN) by gavage (60 mg/ per mouse, dissolved in saline). After 4 h, mice were euthanized for blood collection (200 $\mu$ l), and the fluorescence intensity of FD4 was measured at excitation 485 and 528 emission. The FD4 concentration was calculated using a standard curve.

#### Dual-luciferase reporter assays

The KLB promoters containing the full-length sequence, three 5' truncated fragments, and the TRPV6 promoter were cloned into the GV238 vector (GeneChem, Shanghai, CHN) to construct recombinant luciferase reporter plasmids containing the target gene sequence. Caco2 cells were seeded onto a 24-well plate and were transfected with a plasmid containing the target gene or negative control plasmid (500 ng/well) and Renilla luciferase plasmid (50 ng/well) when cells reached ~70% confluency. 24 h after transfection, the cells were subjected to the indicated treatments. After treatment, the cells were lysed with passive lysis buffer, and luciferase activity was determined with Dual-Luciferase Reporter Assay System kit (Promega cat#E1910). Renilla luciferase was used as an internal reference.

### Chromatin immunoprecipitation (ChIP)

ChIP experiments were performed according to the Magna ChIP™ A/G Kit (Millipore cat#MAGNA0017, MA, USA) standard protocol. Isotype IgG was used as a negative control. Products were finally subjected to RT-PCR.

### Transmission electron microscope (TEM) assay

Cell monolayers were washed with PBS, gently scraped, and centrifuged at 1200 rpm. Cell pellets were fixed with the electron microscopy fixing buffer. Transmission electron microscopy (JEOL, Tokyo, JPN) was used to observe the tight junction ultrastructure of the ultra-thin pellet sections.

### Paracellular permeability assay

Caco2 cells were seeded onto 12-well transwell inserts (0.4 μm pore size; Corning cat#3460, NY, USA). The medium was changed every 2 days until complete cell differentiation (16 days). After differentiation, ethanol (EtOH) or other treatments were performed in cells. The transepithelial electrical resistance (TEER) values were measured and recorded on alternate days.  $TEER = (\text{measured value} - \text{blank value}) \times \text{surface area of the membrane (cm}^2\text{)}$ .

Cells were cultured until a monolayer was formed. Then rinsed with Hank's Balanced Salt Solution (HBSS, Thermo Scientific) and incubated with HBSS containing 0.1 mg/ml FITC-conjugated dextran (4 kDa) (FD-4, MedChemExpress cat#HY-128868A) for one hour. 100 μl of liquid was taken from each of the upper and lower Transwell chambers, and fluorescence was measured using a multi-detection microplate reader with excitation and emission at 480 and 520 nm. Apparent permeability coefficients (Papp) were calculated according to  $Papp (\text{cm s}^{-1}) = (dQ/dt) / (A \times C_0)$ . dQ is the amount of FITC-dextran transported within the dT, A is the initial concentration of FITC-dextran and C<sub>0</sub> is the surface area of the membrane.

### RNA immunoprecipitation (RIP)

We performed the experiments according to the standard protocol of the RNA ChIP-IT Kit (Active Motif cat#53024, Carlsbad, CA, USA), using an isotype IgG antibody as a negative control. Finally, the enrichment of TRPV6 mRNA (3'UTR) was evaluated using RT-PCR.

### Co-immunoprecipitation (Co-IP)

Cells were lysed using RIPA lysis buffer containing protease inhibitor (Beyotime), and the supernatant was collected after centrifugation. The supernatant was precleared for two hours with protein A/G beads (Millipore) and incubated overnight with primary antibodies or IgG control at 4°C. The isolated immunoprecipitates were then analyzed by western blot or Mass Spectrometry (MS).

### Protein stability assay

Cells were treated with 200 μg/mL cycloheximide (CHX, MedChemExpress cat# HY-12320) and harvested at 0, 1, 2, 3, 4 h. Protein expressions were determined by western blot analysis.

### RNA stability assay

Cells were treated with 5 μg/ml actinomycin D (ActD) (Sigma, cat#SBR00013, MO, USA) and collected at different time points. TRPV6 mRNA levels were analyzed by real-time quantitative PCR (RT-PCR).

### Western blot

Ileal tissue or cell samples were added to RIPA lysate buffer containing 1% protease inhibitor (Beyotime) to extract total protein. The primary antibodies against Occludin (Proteintech, dilution ratio 1:1000), ZO-1 (Proteintech, dilution ratio 1:1000), TRPV6 (Proteintech, dilution ratio 1:1000), KLB (Aviva Systems, dilution ratio 1:1000), FXR1 (Proteintech cat#13194-1-AP, RRID: AB\_2110702, dilution ratio 1:1000), HNF4A (Abcam cat#ab181604, RRID: AB\_2890918, dilution ratio 1:1000), Actin (Proteintech, dilution ratio 1:2000) were used. The appropriate HRP-conjugated secondary antibodies (Proteintech, dilution ratio 1:4000) were utilized after overnight incubation of the primary antibodies at 4°C. The antibody validation was provided in the supplemental materials.

### Real-time PCR

According to the manufacturer's protocol, total RNA was isolated from liver and ileum tissues or cells using RNAiso Plus (Takara, Tokyo, JPN), and total RNA was reverse transcribed to yield cDNA using Prime Script™ RT Reagent Kit (Takara). The cDNA was analyzed with Real-Time System (BIO RAD, Berkeley, CA, USA). Relative mRNA levels were calculated by  $\Delta\Delta Ct$  method. Primers used in this study are listed in Supplemental Table 1.

### Bioinformatic analysis

The transcription factors that may bind to the promoter region (-2000 to -1000, -1000 to -350) of the KLB gene were predicted using the transcriptional factor (TF) -Bind online software (<http://tfbind.hgc.jp/>, JPN) and transcription factors were screened out, which bind only in the promoter region of -2000 to -1000. Screening of transcription factors that were highly expressed in the intestinal epithelium from the above transcription factors using Human Protein Atlas software ([www.proteinatlas.org](http://www.proteinatlas.org), SWE).

### Calcium-free medium treatment

Cells were incubated in the DMEM medium (calcium-free) (YuChun, Shanghai, CHN) for 24 h to eliminate the effects of calcium in the medium.

### Measurement of intracellular $[Ca^{2+}]_i$

The intracellular calcium levels were measured using the ratiometric  $Ca^{2+}$  indicator dye Fura2-AM. Cells were seeded in 96-well black polystyrene plates (Corning cat#3916) and incubated with calcium-free medium for 24 h. Then cells were treated with 2.5  $\mu$ M Fura2-AM for 30 min and washed twice. These cells were incubated with calcium-free medium for 10 min and followed by PBS (containing calcium) treatment. Fura2-AM dual excitation and emission was accomplished using 340- and 380-nm excitation filters and a 510 nm emission filter. Fluorescence was measured using a microplate reader (BioTek). The ratio of 340–380 nm fluorescence intensity was recorded as a relative value of intracellular calcium concentration.

### Statistical analysis

Statistical analyses were performed using the statistical package GraphPad Prism v8.0. All results are expressed as mean  $\pm$  SEM. Student's t-tests were used to compare results between two groups, and One-way or Two-way ANOVA were used to compare differences among multiple groups, following with Tukey post-hoc test. Results were considered statistically significant with  $P < 0.05$ .

### Role of funding source

The study was supported by grants from the National Natural Science Foundation of China (81970510, 81873571), Chongqing Natural Science Foundation (cstc2021ycjh-bgzxm0146, cstc2019jcyj-msxmX0336), Talent Project of Chongqing (CQYC201905079) and the Science and Technology Research Program of Chongqing Municipal Education Commission (KJQN201900438). The funders provided financial support but did not participate in the study's design, data collection, data analysis, interpretation, or article writing.

## Results

### Intestinal KLB is reduced in ALD mice

The Lieber-DeCarli diet containing alcohol is widely used to induce ALD models in mice.<sup>34</sup> Compared with the PF mice, alcohol feeding induced hepatic steatosis and inflammatory cell infiltration in C57BL/6 mice (Figure 1a i, ii). The serum transaminases levels and hepatic lipid contents were higher in C57-AF mice livers (Figure 1b and Supplemental Figure 1a, b). The levels of *E. coli* were also increased in the C57-AF group (Supplemental Figure 1c), indicating impairment of the intestinal epithelium barrier. Consistently, the ileal villi of AF mice were sparse and atrophic (Figure 1c i, ii). Immunofluorescent staining also showed a decreased expression

of TJ proteins, Occludin and ZO-1, in the ileal tissues of mice after alcohol feeding (Figure 1c iii-vi), supporting that alcohol feeding disrupted intestinal epithelial barrier integrity. In addition, alcohol feeding did not affect the morphology of the mouse colon (Supplemental Figure 1d). The F4/80 positive cells and the mRNA levels of pro-inflammatory cytokines were elevated in the liver and the ileum of AF mice (Supplemental Figure 1e, f). Interestingly, KLB mRNA and protein levels were downregulated in the intestine of AF mice (Figure 1d), suggesting that the downregulation of intestinal KLB might be involved in ALD development.

Next, we investigated whether and how alcohol regulates KLB expression in Caco2 cells, a widely used intestinal epithelial cell line. Previous studies have demonstrated that 7.5% ethanol (v/v) causes the disruption of the intestinal epithelial TJ barrier in Caco2 cells with no cytotoxicity effects.<sup>35</sup> Here we also observed the effects of different concentrations and different times of ethanol on cell viability and the expression of KLB, ZO-1, and Occludin protein in Caco2 cells. *In vitro*, 24-hour treatment with 5% ethanol (v/v) significantly decreased KLB and TJ protein (Occludin and ZO-1) expression in Caco2 cells and presented minor cytotoxicity (Figure 1e and Supplemental Figure 1g, h). Considering 5% ethanol is far beyond the blood alcohol levels in patients after alcohol consumption, these data may suggest that the epithelial cells in the intestine have been evolutionally adapted to direct alcohol exposure derived from exogenous alcohol absorption and endogenous gut microbial production. Next, dual-luciferase reporter analysis showed that the promoter activities of KLB were decreased after ethanol treatment, suggesting that ethanol might reduce KLB expression via suppressing the KLB promoter activity (Figure 1f). Then the full-length promoter sequence and three 5' truncated promoter fragments of KLB were cloned into a luciferase GV238 vector and transfected into Caco2 cells. Our results showed that the promoter fragment (-2000/-1000) of KLB exhibited the highest activity among all truncated fragments in Caco2 cells, while the promoter fragment (-1000/-350) showed a suppressed activity (Figure 1g).

Next, we used TFbind software and the Human Protein Atlas online database to screen potential TF candidates (Figure 1h). The expression of three TF candidates, homeobox protein CDX-1 (CDX1), hepatocyte nuclear factor 1-alpha (HNF1A) and HNF4A, was measured in ethanol-treated cells. Interestingly, ethanol only downregulated HNF4A expression in Caco2 cells (Figure 1h). Western blot analysis further showed that ethanol down-regulated the expression of HNF4A protein *in vivo* and *in vitro* (Figure 1i). In addition, treatment with Benfluorex, an agonist of HNF4A, elevated the promoter luciferase activity and the protein levels of KLB in Caco2 cells in the absence and presence of ethanol (Figure 1j, k). Moreover, as predicted by JASPAR

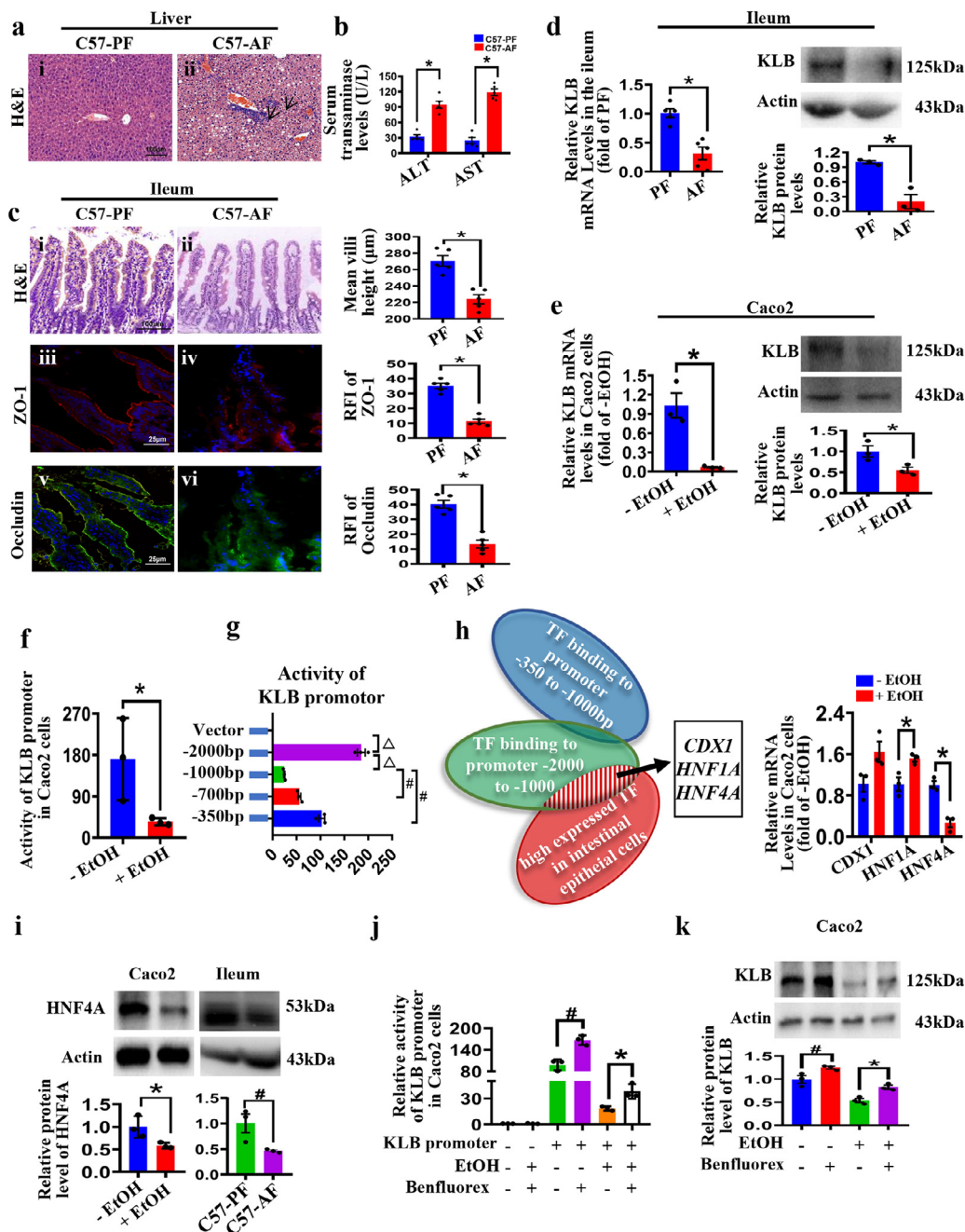


**Figure 1. Alcohol decreases intestinal KLB expression by inhibiting HNF4A.** C57BL/6 mice were fed with alcohol or paired Lieber DeCarli diet for 28 days ( $n=5$ ). (a) Pathological changes of mice livers. Representative images of H&E staining (i-ii, arrows indicate inflammatory cells infiltration). (b) Serum levels of ALT and AST. (c) Representative H&E staining (i-ii) and immunofluorescence staining of ZO-1 (iii-iv, red) and Occludin (v-vi, green) in the ileal tissues. (d) The mRNA ( $n=5$ ) and protein ( $n=3$ ) levels of KLB in the ileum of mice. \*  $P<0.05$  vs. PF mice. (e) The mRNA and protein levels of KLB in Caco2 cells treated with or without EtOH for 24h ( $n=3$ ). (f, g) The activity of KLB promoter in Caco2 cells ( $n=3$ ). \*  $P<0.05$  vs. (-)EtOH group,  $\Delta$   $P<0.05$  vs. -2000bp group; #  $P<0.05$  vs. -1000bp group. (h) The candidate transcription factors in regulating KLB and the mRNA levels of the three transcription factors were measured in Caco2 cells treated with EtOH ( $n=3$ ). \*  $P<0.05$  vs. (-)EtOH. (i) The protein level of HNF4A in Caco2 cells and ileum ( $n=3$ ). \*  $P<0.05$  vs. (-)EtOH; #  $P<0.05$  vs. PF mice. (j, k) The activity of KLB promoter (j) and the protein level of KLB (k) in benfluorex-treated cells ( $n=3$ ). #  $P<0.05$  vs. EtOH(-)/Benfluorex(-) group; \*  $P<0.05$  vs. EtOH(+)/Benfluorex(-) group. Statistical analysis was performed using one-way ANOVA followed with Tukey post-hoc test or t-test. Data are mean  $\pm$  SEM. AF, alcohol-fed; PF, pair-fed.

bioinformatics software, there were two HNF4A binding sites on the KLB promoter (S1 and S2) (Supplemental Figure 1i). ChIP assays demonstrated that S1 is the primary site where HNF4A binds to the KLB promoter (Supplemental Figure 1i). These data suggested that ethanol decreased KLB promoter activity through inhibiting HNF4A, and hence down-regulated KLB expression in enterocytes.

#### Intestine-specific KLB overexpression protects mice from ALD

Next, we constructed a mouse model of enterocytes-specific KLB overexpression based on the FLEX-ON system. Two weeks after tail vein injection, the mice were randomly divided into four groups: AAV-NC-PF, AAV-NC-AF, AAV-KLB-PF, AAV-KLB-AF, and were fed with alcohol or Pair diet for 4 weeks (Figure 2a).

Immunofluorescent staining confirmed that AAV-Flag protein was upregulated in the intestinal epithelium but not in the liver of AAV-KLB mice (Supplemental Figure 2a). RT-PCR and western blot analysis further confirmed that KLB protein was upregulated in the ileum of AAV-KLB mice with or without alcohol (Figure 2b, c). In addition, the mRNA levels of KLB were not increased in the liver (Supplemental Figure 2b), supporting the successful construction of an intestine-specific KLB overexpression mouse model.

Notably, the liver-to-body weight ratio and serum levels of ALT in the circulation and LPS levels in the portal vein were lower in AAV-KLB-AF mice than in AAV-NC-AF mice (Figure 2d-f). The body weight lost was alleviated in the AAV-KLB-AF mice compared to AAV-NC-AF mice (Supplemental Figure 2c). AAV-KLB-AF mice displayed apparently attenuated liver steatosis and inflammatory cell infiltration as evidenced by H&E, Oil red O staining and the quantitative TG measurements compared to AAV-NC-AF mice (Figure 2g i-viii). Hepatic accumulation of F4/80 positive cells and the translocation of bacterial products induced by alcohol treatment were attenuated in AAV-KLB-AF mice. (Figure 2g ix-xvi). Consistently, the mRNA levels of lipogenesis genes (FAS and SCD-1) and pro-inflammatory cytokines (IL-1 $\beta$ , IL-6 and TNF- $\alpha$ ) were decreased in AAV-KLB-AF mice (Supplemental Figure 2d). Thus, our data support that enterocyte-specific overexpression of KLB could protect mice from alcohol-induced liver steatosis and inflammation.

#### Intestine-specific KLB overexpression protects mice from alcohol-induced intestinal epithelial barrier impairment

We further evaluated the intestinal morphology of AAV-KLB mice. The ileal villi of AAV-KLB-AF mice were more densely arranged than AAV-NC-AF mice (Figure 3a). Meanwhile, F4/80 positive cells infiltration in the ileum of mice were attenuated in the AAV-KLB-AF mice compared with the AAV-NC-AF mice

(Figure 3b). Goblet cells are single-cell glands whose main function is to synthesize and secrete mucins forming a mucosal barrier to protect epithelial cells. KLB overexpression attenuated alcohol-induced decrease of the goblet cells and the mucosal barrier (Figure 3c, d). The expression of Occludin and ZO-1 was also upregulated in the intestine of AAV-KLB-AF mice compared to that in AAV-NC-AF mice (Figure 3e-g). In order to evaluate intestinal permeability, the concentrations of serum FD<sub>4</sub> in AAV-KLB-AF mice was lower than in AAV-NC-AF mice (Figure 3h). In addition, the forced upregulation of intestinal KLB suppressed the ileal expression of inflammatory factors (IL-1 $\beta$ , IL-6 and TNF- $\alpha$ ) and promoted the ileal expression of defensin beta 1 (DEFB1), cathelicidin-related antimicrobial peptide (CRAMP) and Leucine-rich repeats and immunoglobulin-like domains protein 1 (Lrig1) in mice with AF treatment (Supplemental Figure 2e). These data indicate that enterocyte-specific overexpression of KLB protects mice from alcohol-induced intestinal epithelial barrier impairment.

#### KLB regulates the intestinal epithelial barrier and the expression of ZO-1/Occludin on plasma membranes in Caco2 cells

We firstly established an *in vitro* model of polarized monolayer intestinal epithelial barrier using Caco2 cell (Supplemental Figure 3a, b), as previously described.<sup>36</sup> The paracellular permeability assay showed that 5% (v/v) of ethanol reduced the TEER values and increased Papp values in the polarized monolayer intestinal epithelial barrier (Supplemental Figure 3c). In accordance with this, ethanol treatment decreased the expression of Occludin and ZO-1 and severely disrupted their membrane distribution in the Caco2 cells (Supplemental Figure 3d, e). Importantly, KLB overexpression remarkably reversed the ethanol-changed TEER and Papp values in Caco2 transwell inserts (Figure 4a). Tight junctions were also more compacted in KLBOE cells as observed via TEM (Figure 4b). The expression and membrane distribution of Occludin and ZO-1 in KLBOE cells were also increased with or without ethanol treatment (Figure 4c, d). In addition, overexpression of KLB did not increase the mRNA levels of Occludin and ZO-1 in Caco2 cells (Supplemental Figure 3f). Then protein stability analysis demonstrated that KLB overexpression increased the protein stability of Occludin and ZO-1, suggesting KLB regulated the levels of Occludin and ZO-1 via enhancing their protein stability (Figure 4e).

Then siRNA against KLB was transfected into Caco2 cells and the KLB expression was stably inhibited until 48h after transfection (Figure 4f and Supplemental Figure 3g). Inhibition of KLB (KLBi) elevated the permeability of the epithelial barrier as indicated by the decreased TEER values and increased Papp values (Figure 4f). KLBi also remarkably decreased the expression of Occludin and ZO-1 and weakened their

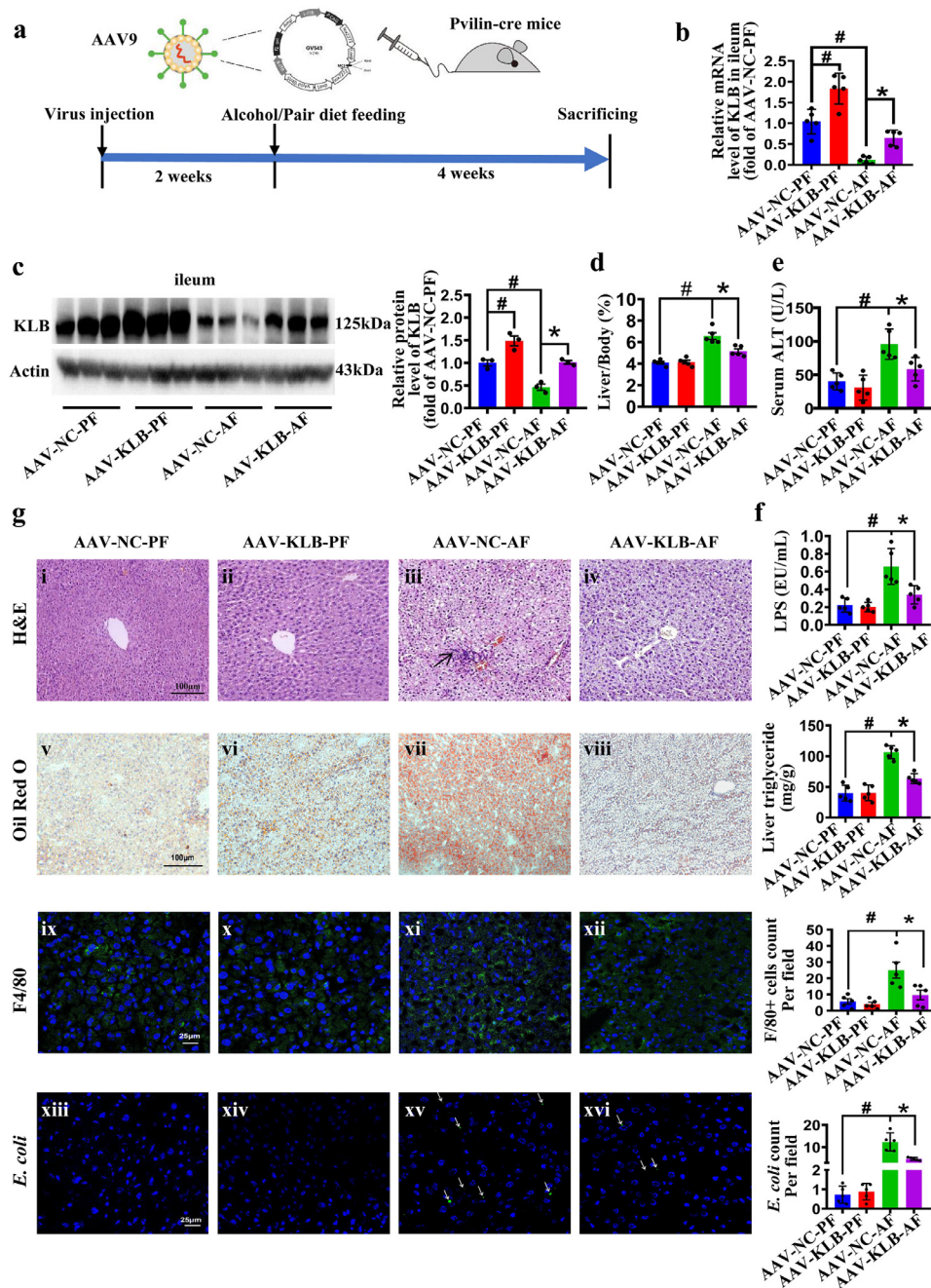


**Figure 2. Intestine-specific KLB overexpression protects mice from ALD.** (a) AAV9-FLEX-KLB-3Flag or AAV9-FLEX-NC-3Flag vectors were injected into Pvalin-cre mice to construct the enterocytes-specific KLB overexpression (AAV-KLB) or negative control (AAV-NC) mice, and then these mice were randomly assigned to receiving alcohol or paired diet for 4 weeks ( $n=5$ ). (b, c) The mRNA ( $n=5$ ) (b) and protein ( $n=3$ ) (c) levels of KLB in mice ileum. (d) The ratio of liver-to-body-weight. (e, f) The levels of serum ALT (e) and portal vein serum LPS (f). (g) Pathological changes of mice livers. Representative images of Oil Red O staining of neutral lipid in the livers (v-viii) and quantification of hepatic triglyceride content of mice. Representative images of F4/80 staining (ix-xii, green) and *E. coli* immunofluorescence staining (xiii-xvi, green, arrows indicate *E. coli* infiltration). #  $P < 0.05$  vs. AAV-NC-PF; \*  $P < 0.05$  vs. AAV-NC-AF. Statistical analysis was performed using one-way ANOVA followed with Tukey post-hoc test. Data are mean  $\pm$  SEM. AAV-NC, adeno-associated virus-negative control; AAV-KLB, adeno-associated virus-KLB overexpression; AF, alcohol-fed; PF, pair-fed.

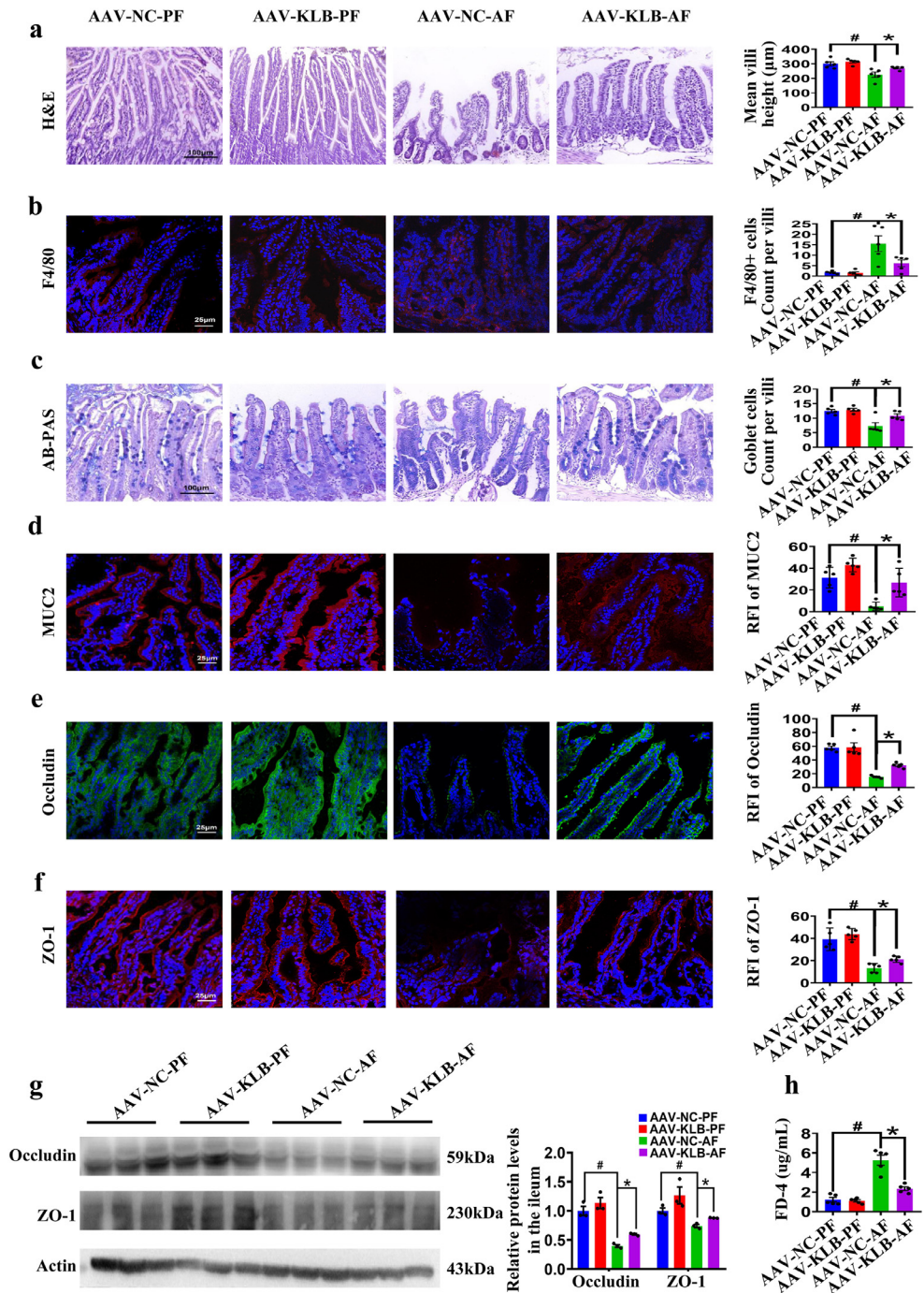


**Figure 3. Intestine-specific KLB overexpression protects mice from alcohol-induced intestinal epithelial barrier impairment.** (a) Representative images of H&E staining of the ileal tissues and the quantification of villi height ( $n=5$ ). (b) Representative images of F4/80 staining (red) of the ileal tissues and the quantification of F4/80 positive cells. (c) Representative images of AB-PAS staining (blue) and quantification of goblet cells. (d) Representative images of MUC2 immunofluorescence staining (red) and the quantitative RFI of MUC2. (e, f) Representative images of the Occludin (e, green) and ZO-1 (f, red) immunofluorescence staining in the ileal tissues. (g) The protein level of Occludin and ZO-1 in the ileal tissues ( $n=3$ ). (h) The serum levels of FD4 ( $n=5$ ). #  $P < 0.05$  vs. AAV-NC-PF; \*  $P < 0.05$  vs. AAV-NC-AF. Statistical analysis was performed using one-way ANOVA followed with Tukey post-hoc test. Data are mean  $\pm$  SEM. AAV-NC, adeno-associated virus-negative control; AAV-KLB, adeno-associated virus-KLB overexpression; AF, alcohol-fed; PF, pair-fed; RFI, relative fluorescence intensity; FD4, fluorescein isothiocyanate (FITC)-dextran 4000MW.

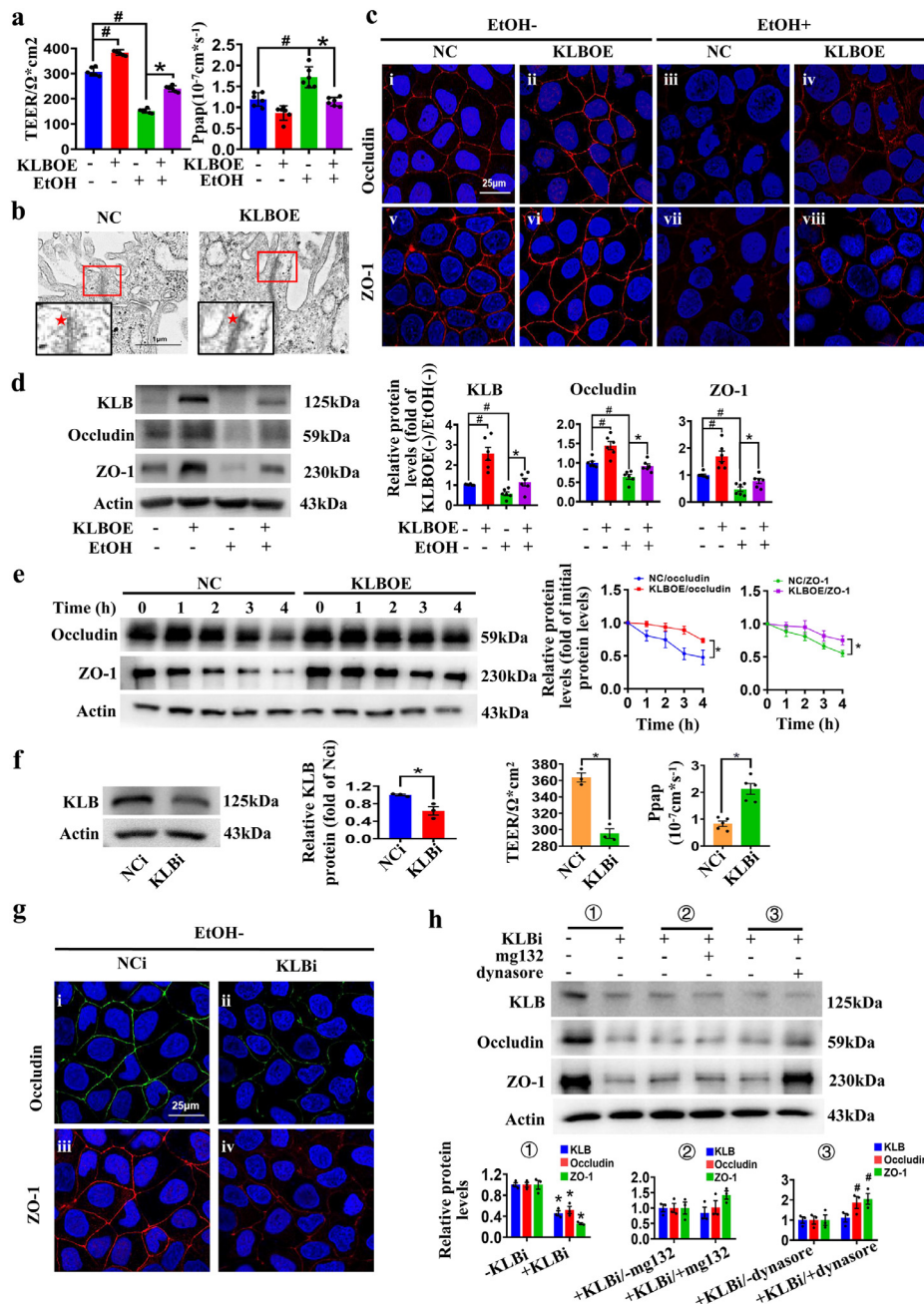


**Figure 4. The protective effects of KLB on the intestinal barrier.** (a) TEER and Papp values of KLBOE and NC cells treated with EtOH for 24h ( $n=6$ ). (b) Representative images of transmission electron microscope images of the tight junction structures (indicated by red star) in KLBOE and NC cells ( $n=4$ ). (c) Representative images of immunofluorescence staining of Occludin (i-iv, red) and ZO-1 (v-viii, red) in KLBOE and NC cells treated with EtOH for 24 h ( $n=3$ ). (d) The protein levels of Occludin and ZO-1 in KLBOE and NC cells were measured by western blot ( $n=6$ ). #  $P < 0.05$  vs. KLBOE(-)/EtOH(-); \*  $P < 0.05$  vs. KLBOE(-)/EtOH(+). (e) The NC or KLBOE cells were harvested at the indicated time points after CHX treatment, and protein levels were analyzed by western blot ( $n=6$ ). \*  $P < 0.05$  vs. NC cells. (f) The protein level of KLB ( $n=3$ ), TEER values ( $n=3$ ) and Papp ( $n=5$ ) values of NCi and KLBi cells. \*  $P < 0.05$  vs. NCi cells. (g) Representative images of immunofluorescence staining of Occludin (i-ii, green) and ZO-1 (iii-iv, red) in NCi and KLBi cells ( $n=3$ ). (h) The expression of Occludin and ZO-1 in MG-132 or Dynasore treated NCi and KLBi cell ( $n=3$ ). \*  $P < 0.05$  vs. (-)KLBi; #  $P < 0.05$  vs. (+)KLBi/(-) dynasore. Statistical analysis was performed using one-way/two-way ANOVA followed with Tukey post-hoc test or t-test. Data are mean  $\pm$  SEM. TEER, transepithelial electrical resistance; Papp, apparent permeability coefficient; NC, negative control; NCi, negative control for RNA interference; KLBOE, KLB overexpression; KLBi, inhibition of KLB.

membrane distribution (Figure 4g). To determine the mechanism by which KLBI reduces the expression levels of Occludin and ZO-1, different concentrations of Dynasore, an inhibitor of endocytosis, and MG132 (proteasome inhibitor) were used to treat Caco2 cells transfected with KLB siRNA, respectively (Supplemental Figure 4a, b). Dynasore reversed the KLBI-induced decrease in TJ proteins, while there was no difference between cells with or without MG132 treatment (Figure 4h and Supplemental Figure 4a, b), indicating that KLB regulated Occludin and ZO-1 degradation via endocytosis rather than ubiquitin-proteasome pathway. These data suggest that KLB regulates the intestinal epithelial barrier by regulating the endocytosis and degradation of TJ proteins.

#### TRPV6 is necessary for KLB regulating the endocytosis of TJ proteins

TRPV6 interacts with endocytosis-related proteins such as Numb1 and clathrin, and colocalizes with early endosomal antigen, suggesting that it may play a role in endocytosis.<sup>37,38</sup> As shown in Figure 5a, TRPV6 expression was decreased after ethanol treatment, and KLBOE promoted TRPV6 expression while KLBI inhibited its expression in Caco2 cells. Immunofluorescence staining of TRPV6 on the plasma membrane of Caco2 cells showed the same changes (Figure 5b). Likewise, the ileal TRPV6 expression was decreased in AF mice, and the forced upregulation of KLB upregulated TRPV6 expression *in vivo* (Supplemental Figure 4c). Next, the TRPV6 siRNA or TRPV6 overexpression plasmid was transfected into KLBOE cells or KLBI Caco2 cells. Inhibition of TRPV6 (TRPV6i) decreased the protein levels and plasma membrane distributions of Occludin and ZO-1 in KLBOE cells, while overexpression of TRPV6 (TRPV6OE) restored the decreased expression and weakened plasma membrane distributions of Occludin and ZO-1 caused by KLBI (Figure 5c, d). The measurements of TEER values and Papp values further indicated that inhibition of TRPV6 disrupts the epithelial barrier in KLBOE cells and overexpression of TRPV6 enhances the epithelial barrier in KLBI cells (Figure 5e, f). These results clearly demonstrate that KLB regulates intestinal TJ proteins via TRPV6.

We then investigated whether TRPV6 directly interacts with TJ proteins and KLB. As evidenced by the data from Co-IP and confocal microscope, TRPV6 could form a protein complex with Occludin, ZO-1 and KLB (Figure 6a, b). Inhibition of KLB suppressed the interaction between TRPV6 and TJ proteins, and KLB overexpression promoted this interaction (Figure 6c), indicating that KLB regulates the formation of TRPV6/TJ proteins complex. Next, the TRPV6 overexpression plasmid or TRPV6 siRNA was transfected into Caco2 cells and the expression of TRPV6 was stably modulated without concomitant modulation of KLB (Supplemental Figure 5a, b). While the overexpression of TRPV6 alone

promoted protein stability of Occludin and ZO-1, the inhibition of TRPV6 alone reduced stability of these proteins, compared with their respective controls (Figure 6d). Consequently, the protein levels were upregulated in TRPV6OE cells and downregulated in TRPV6i cells (Supplemental Figure 5c, d). These results suggest that TRPV6 directly modulates the protein stability of TJ proteins (Occludin and ZO-1).

Then Dynasore was added to CHX-treated TRPV6i cells, and the results showed that the blockade of endocytosis increased protein stability of Occludin and ZO-1 in TRPV6i cells (Figure 6e). Consistently, the expression of Occludin and ZO-1 were increased in Dynasore-treated TRPV6i cells (Supplemental Figure 5e). In addition, to directly observe the effect of TRPV6 on the endocytosis of TJ proteins, Rab5, a master regulator of endocytic processes, was co-stained with Occludin and ZO-1. The confocal images showed that inhibition of TRPV6 promoted Occludin and ZO-1 endocytosis, and the ethanol-induced endocytosis of TJ proteins was restored by TRPV6 overexpression (Figure 6f). These data further support that TRPV6 regulates endocytosis and degradation of TJ proteins in the enterocytes.

Since TRPV6 was previously identified to be associated with Ca<sup>2+</sup> homeostasis in the gut,<sup>24</sup> we also examined whether TRPV6 regulates TJ proteins in a calcium-dependent manner in Caco2 cells. However, in the present study, TRPV6 overexpression did not change intracellular calcium levels (Supplemental Figure 6a). Culturing cells with Ca<sup>2+</sup>-free medium also did not affect ZO-1 and Occludin expression in TRPV6OE cells (Supplemental Figure 6b). These data suggest that the regulation of TRPV6 on TJ proteins expression is independent of its calcium ion channel activity.

#### KLB interacts with FXR1 to regulate TRPV6 mRNA stability

To further explore the mechanism by which KLB regulates TRPV6, we tested the mRNA levels of TRPV6 in the ethanol treatment, KLBI and KLBOE groups. The results showed that ethanol or KLBI decreased TRPV6 mRNA, and KLBOE increased TRPV6 mRNA (Figure 7a). However, the dual-luciferase reporter assay showed no difference in promoter activity between the KLBOE and NC groups (Figure 7b). RNA stability assay showed that the mRNA stability of TRPV6 in the KLBOE group was higher than that in the NC group, indicating that KLB regulates the mRNA stability of TRPV6 (Figure 7c).

Since RNA-binding proteins are important regulators of mRNA stability, RNA-binding proteins bound to KLB were then screened by MS, and FXR1, an mRNA stability regulator, was verified to interact with KLB by RIP (Figure 7d). As our data showed, the relative enrichment of TRPV6 mRNA (3'UTR) in FXR1 protein was decreased in KLBOE cells, compared with the NC group (Figure 7e). We then established a FXR1 protein

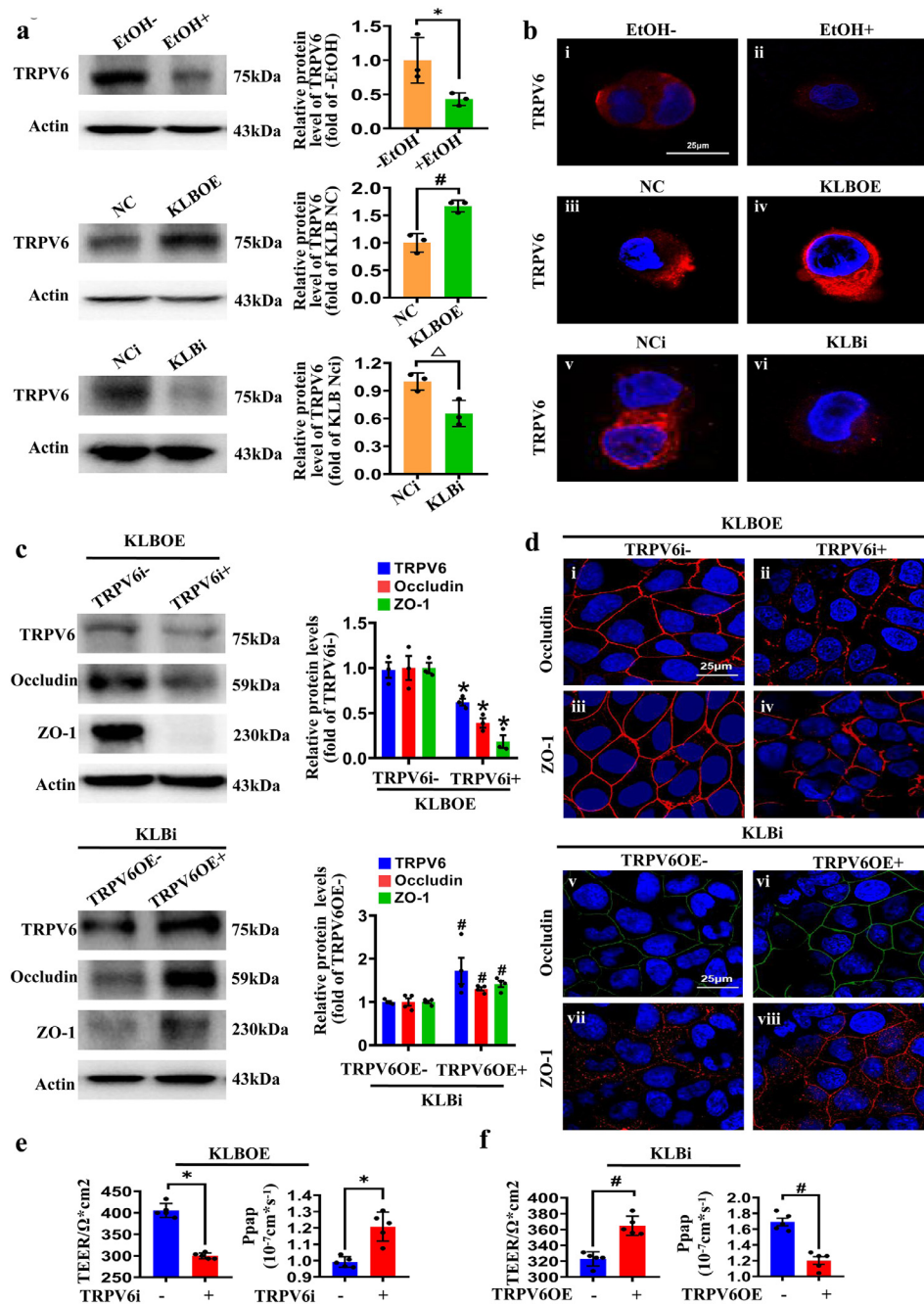


**Figure 5. TRPV6 is necessary for KLB regulating TJ proteins.** (a) The protein levels of TRPV6 in the EtOH-treated cells, KLBOE group and KLBi group ( $n=3$ ). \*  $P < 0.05$  vs. (-)EtOH; #  $P < 0.05$  vs. KLB NC;  $\Delta$   $P < 0.05$  vs. KLB NCi. (b) Representative images of immunofluorescence of TRPV6 (red) in EtOH treated Caco2 cells (i-ii), KLBOE cells (iii-iv) and KLBi cells (v-vi) ( $n=3$ ). (c) The protein levels of Occludin and ZO-1 in KLBOE cells with or without TRPV6i (upper panel,  $n=3$ ), and Occludin/ZO-1 expression in KLBi cells with or without TRPV6OE (lower panel,  $n=4$ ). (d) Representative images of immunofluorescence of Occludin and ZO-1 in KLBOE cells with or without TRPV6i (i-iv), and in KLBi cells with or without TRPV6OE (v-viii) ( $n=3$ ). (e, f) TEER and Papp values in KLBOE cells with or without TRPV6i (e) and in KLBi cells with or without TRPV6OE (f),  $n=5$ . \*  $P < 0.05$  vs. KLBOE(+)/TRPV6i(-); #  $P < 0.05$  vs. KLBi(+)/TRPV6OE(-). Statistical analysis was performed using t-test. Data are mean  $\pm$  SEM. TEER, transepithelial electrical resistance; Papp, apparent permeability coefficient; NC, negative control; NCi, negative control for RNA interference; KLBOE, KLB overexpression; KLBi, inhibition of KLB; TRPV6OE, TRPV6 overexpression; TRPV6i, inhibition of TRPV6.

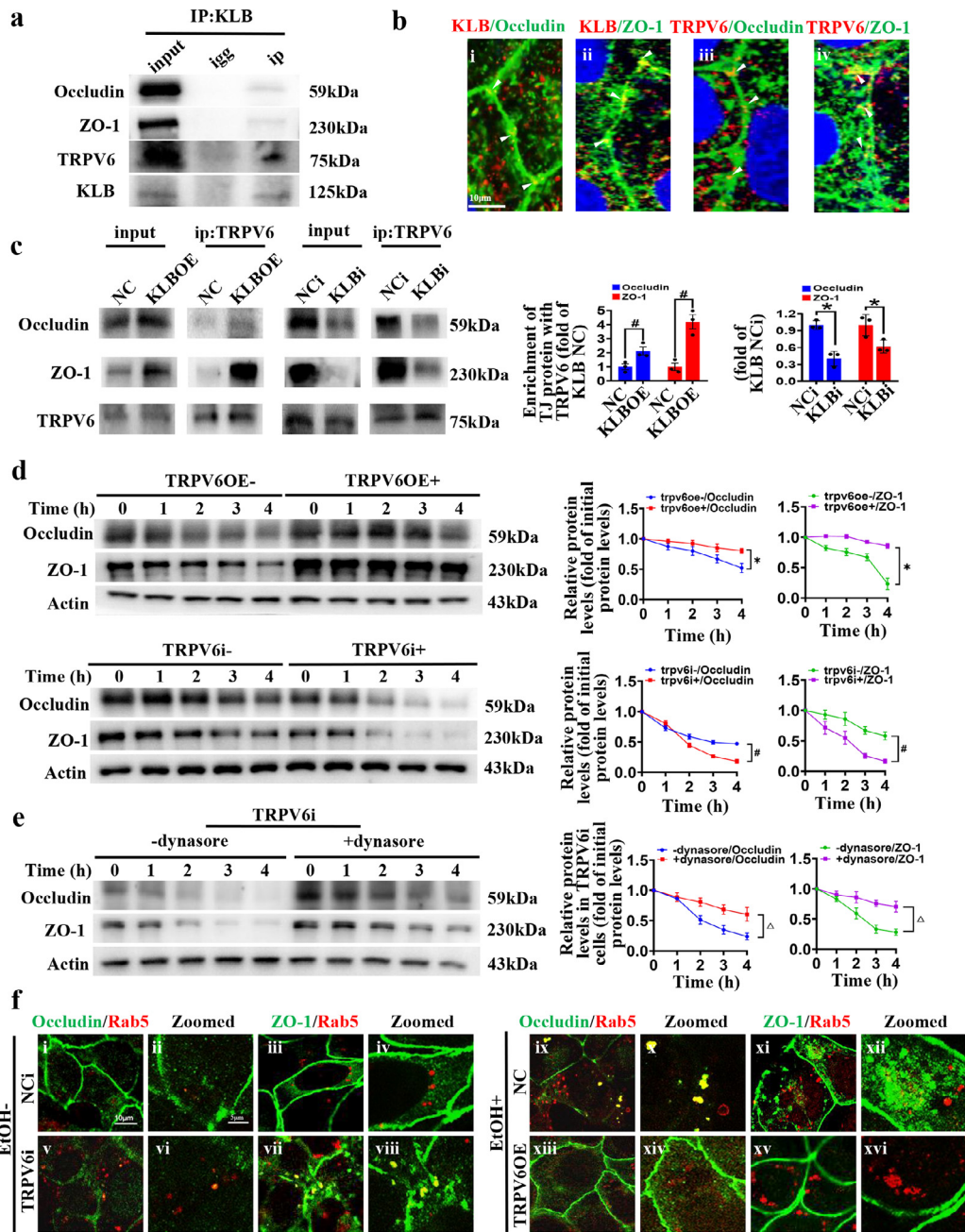


**Figure 6. TRPV6 regulates the protein stability of Occludin and ZO-1 via the endocytic pathway.** (a) The interactions between KLB, TRPV6 and Occludin/ZO-1 were detected by Co-IP ( $n=3$ ). (b) Representative confocal images of co-localization (yellow point, indicated with white arrow) between KLB (red) and Occludin/ZO-1 (green), (i, ii) or the co-localization between TRPV6 (red) and Occludin/ZO-1 (green), (iii, iv),  $n=4$ . (c) The interaction between TRPV6 and Occludin/ZO-1 was detected by Co-IP in KLBOE or KLBi cells ( $n=3$ ). #  $P<0.05$  vs. KLB NC; \*  $P<0.05$  vs. KLB NCI. (d) The protein stabilities of Occludin and ZO-1 in the TRPV6OE cells or TRPV6i cells ( $n=6$ ). \*  $P<0.05$  vs. TRPV6OE(-); #  $P<0.05$  vs. TRPV6i(-). (e) The protein stability assays of Occludin and ZO-1 in TRPV6i cells treated with or without Dynasore ( $n=6$ ).  $\Delta$   $P<0.05$  vs. (-)dynasore. (f) Representative confocal images of co-localizations (yellow) between Occludin/ ZO-1 (green) and Rab5 (red) in NCI (i-iv)/TRPV6i (v-viii) or NC (ix-xii)/TRPV6OE cells (xiii-xvi),  $n=4$ . Statistical analysis was performed using one-way/two-way ANOVA followed with Tukey post-hoc test or t-test. Data are mean  $\pm$  SEM. NC, negative control; NCI, negative control for RNA interference; KLBOE, KLB overexpression; KLBi, inhibition of KLB; TRPV6OE, TRPV6 overexpression; TRPV6i, inhibition of TRPV6.

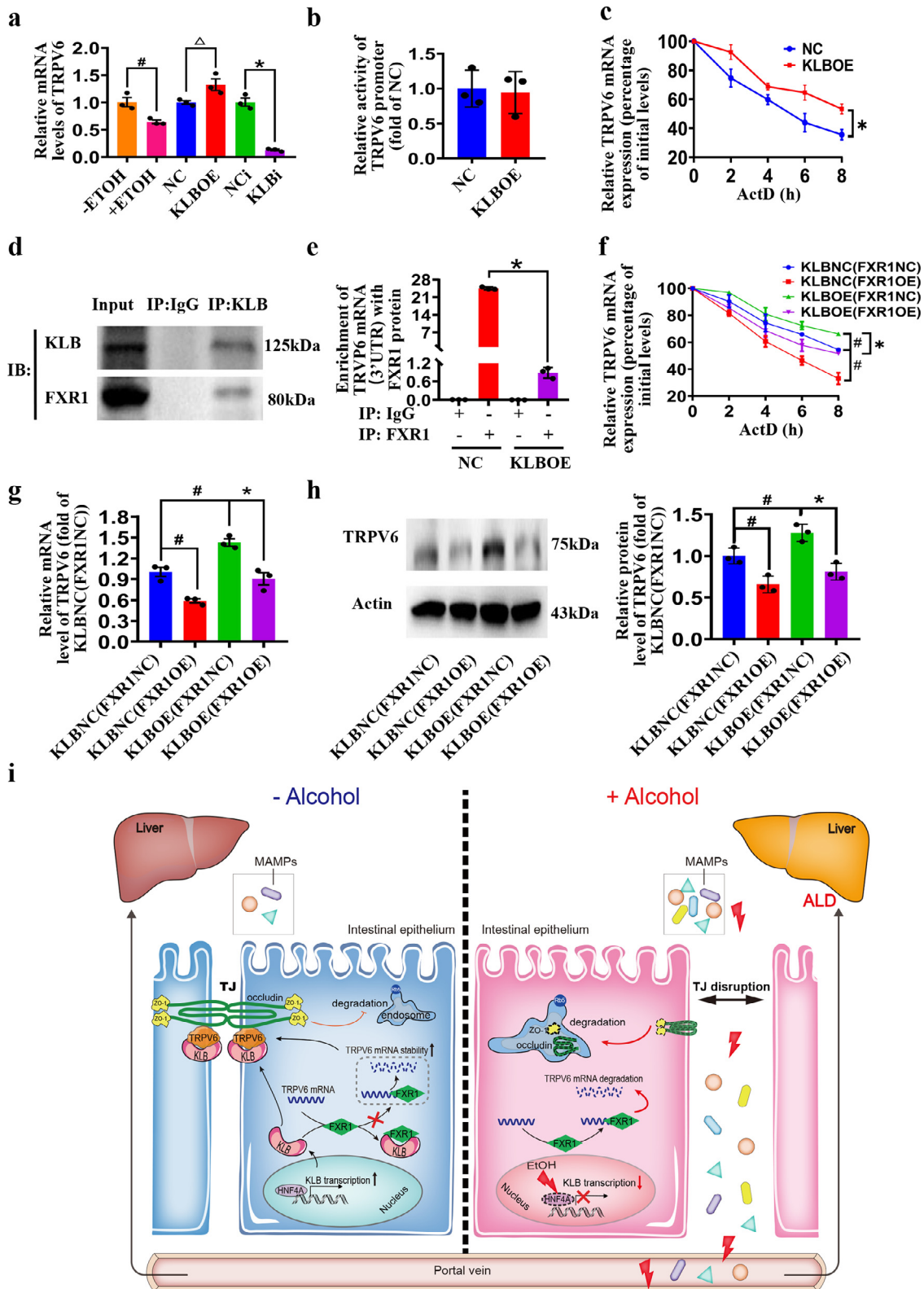


**Figure 7. KLB interacts with FXR1 to regulate TRPV6 mRNA stability.** (a) The mRNA levels of TRPV6 in EtOH treated Caco2 cells, KLBOE cells, and KLBi cells.  $n=3$ , #  $P<0.05$  vs. (-)EtOH;  $\Delta$   $P<0.05$  vs. KLB NC; \*  $P<0.05$  vs. KLB NCi. (b) The activity of TRPV6 promoter

overexpressing (FXR1OE) cell line in the background of KLBOE or NC. The RNA stability analysis showed that FXR1OE decreased the stability of TRPV6 mRNA in both KLB NC and KLBOE cells (Figure 7f). In addition, the elevated TRPV6 mRNA stability in KLBOE cells can be reversed by FXR1 overexpression (Figure 7f). Our results also verified that FXR1OE downregulated the mRNA level and protein expression of TRPV6 in both NC and KLBOE cells (Figure 7g, h).

### Discussion

Growing evidence indicates that compromised intestinal barrier function is closely related to the development and progression of ALD.<sup>39</sup> Unfortunately, most clinical data are correlative, making it difficult to separate the cause from effect in interpreting the importance of barrier loss. In the present study, using experimental animal models, we present new insights into the significance of the intestinal epithelial barrier in ALD. While alcohol consumption decreases intestinal KLB expression, enterocyte-specific overexpression of KLB could protect mice from alcohol-induced intestinal epithelial barrier impairment, thereby ameliorating ALD.

HNF4A is an essential TF in the development of the colon as well as the maintenance of adult gut physiology.<sup>40</sup> Intestinal epithelial cell-specific HNF4A-null mice showed lower expression of several genes including mucins and aquaporins, as well as an elevated histological inflammatory state, resulting in increased intestinal permeability and susceptibility to DSS-induced IBD.<sup>41</sup> The alcohol-induced intestinal dysbiosis may also contribute to the decrease of HNF4A expression in the intestine.<sup>39,42</sup> Studies demonstrated that alcohol causes intestinal dysbiosis, which also contributes to the decrease of HNF4A expression in the intestine.<sup>39,42</sup> *In vivo* and *in vitro*, we found that the mRNA and protein levels of intestinal KLB were decreased by alcohol. Next, we screened and validated HNF4A as a TF which can bind to KLB promoter, regulating its expression. We further demonstrated that alcohol decreased intestinal HNF4A expression both *in vivo* and *in vitro*. Benfluorex, an agonist of HNF4A, increased the expression of KLB in the presence or absence of alcohol. These data suggest that the inhibition of HNF4A is a key regulatory mechanism for alcohol-induced downregulation of KLB expression in intestinal epithelial cells.

Furthermore, our data showed that intestine-specific KLB upregulation protected mice from alcohol-induced intestinal epithelial barrier impairment, thereby alleviating liver steatosis and inflammation. KLB was previously considered as an essential reservoir for FGF21 binding to the extracellular matrix and as a co-receptor of FGFR21 signaling.<sup>43</sup> FGF21 plays an important role in regulating energy balance and alcohol metabolism. While FGF21 deficiency exacerbates alcohol-induced intestinal permeability and liver injury,<sup>44,45</sup> the exogenous FGF21 administration could protect the liver from chronic alcohol-induced injury.<sup>46</sup> Interestingly, in the present study, we found that KLB overexpression improves intestinal epithelial hyperpermeability in alcohol-treated Caco2 cells without FGF21 treatment, suggesting the role played by KLB extends far beyond a co-receptor of FGF21 pathway.

It is well-known that alcohol-induced intestinal epithelial barrier impairment is strongly correlated with a decrease in TJ proteins and hence disruption of TJ structures.<sup>47</sup> Occludin and ZO-1 are the two major components of tight junctions in intestinal epithelial cells. Gastric epithelium hyperplasia was found in Occludin<sup>-/-</sup> mice, with the loss of chief and parietal cells, and with increased aberrant mucoid-containing cells, thickened gastric mucosa and severe inflammatory infiltrates.<sup>48</sup> In humans, mutations in the OCLN gene encode an unfunctional Occludin protein in neurovascular and cerebral endothelial, causing an increase in blood-brain barrier permeability.<sup>49</sup> Some *in vitro* experiments confirmed that ZO-1 depletion delayed TJ formation.<sup>50,51</sup> In the present study, we observed that intestinal-specific overexpression of KLB negatively regulates intestinal epithelial barrier permeability and it has no significant effect on alcohol consumption. Consistently, KLB inhibition decreased the expression of TJ proteins (Occludin and ZO-1) on the plasma membranes of Caco2 cells, while KLB overexpression increased their expression on plasma membranes even in the presence of alcohol.

Interestingly, KLB seems to regulate the endocytosis and degradation of Occludin and ZO-1, rather than regulating their mRNA levels or ubiquitin-proteasome degradation. Endocytosis of TJ proteins from the plasma membrane is a key mechanism regulating TJ plasticity and function in epithelial barrier tissues.<sup>52</sup> Previous studies have shown that alcohol could enhance intestinal Occludin endocytosis and degradation causing

in NC and KLBOE cells. (c) The TRPV6 mRNA stability in NC and KLBOE cells in the presence of ActD.  $n=3$ , \*  $P<0.05$  vs. KLB NC. (d) The Co-IP of KLB and FXR1 ( $n=3$ ). (e) Relative enrichment of TRPV6 mRNA 3'UTR in FXR1 protein of NC and KLBOE cells.  $n=3$ , \*  $P<0.05$  vs. KLB NC. The KLBOE or KLBNC cells were transfected with FXR1 overexpression (FXR1OE) or control plasmid (FXR1NC), respectively. (f) The mRNA stability of TRPV6, the mRNA levels (g) and protein levels of TRPV6 (h) in these cells.  $n=3$ , #  $P<0.05$  vs. KLBNC(FXR1NC); \*  $P<0.05$  vs. KLBOE(FXR1NC). Statistical analysis was performed using one-way/two-way ANOVA followed with Tukey post-hoc test or t-test. Data are mean  $\pm$  SEM. (i) The Schematic diagram for the mechanisms of alcohol reduces intestinal KLB expression via HNF4A, resulting in intestinal barrier disruption and subsequent liver injury. The intestinal KLB could interact with FXR1 to enhance TRPV6 mRNA stability, inhibiting the endocytosis and degradation of tight junction proteins. NC, negative control; NCi, negative control for RNA interference; KLBOE, KLB overexpression; KLBi, inhibition of KLB; ActD, actinomycin D.

diarrhea.<sup>53</sup> ZO-1 endocytosis is also involved in TJ decomposition in kidney epithelial cells.<sup>54</sup>

TRPV6 belongs to the transient receptor potential vanilloid (TRPV) family, which consists of six members: TRPV1-6. Structurally, TRPVs contain six transmembrane spanning ion channels characterized by N-terminal ankyrin repeats and a C-terminal TRP domain. A recent study suggested that transient receptor potential vanilloid subtype 1 (TRPV1), the most studied member of the TRPV channel family, plays a role in binding SARS-CoV-2 through the interaction between these ankyrin repeats domain of TRPV1 and the ankyrin binding motifs of SARS-CoV-2 S protein.<sup>55</sup> In leukemia cells, TRPV6 combined with lymphocyte-specific protein tyrosine kinase (Lck) located at cell membranes and uncoupled the combination would allow Lck to depart from the plasma membrane into the cytosol.<sup>56</sup> These data suggest that TRPV6 may play a role in regulating protein-protein interactions.

Consistently, our data showed that there was a complex comprising TRPV6, Occludin, ZO-1 and KLB in intestinal epithelial cells and KLB positively modulated the interaction between TRPV6 and TJ proteins. Furthermore, the inhibition of TRPV6 reduced the expression of Occludin and ZO-1 in KLBOE cell plasma membranes, and the overexpression of TRPV6 restored the decreased expression in KLBi cells, supporting TRPV6 is necessary for KLB regulating TJ proteins expression. In addition, TRPV6 alone regulated the endocytic degradation of Occludin and ZO-1 in Caco2 cells. Thus, these data support that KLB positively regulates TJ protein expression via TRPV6-mediated endocytic degradation pathway. Further studies are needed to confirm the role of TRPV6 *in vivo*.

Moreover, our data showed that KLB regulated TRPV6 expression by modulating mRNA stability. Using IP-MS and Co-IP approaches, we found that KLB could interact with FXR1. FXR1 is an important RNA-binding protein that plays a critical role in RNA metabolism.<sup>57</sup> In prostate cancer cells, FXR1 binds to the 3'UTR of F-box protein 4 to induce its mRNA degradation.<sup>58</sup> FXR1 also negatively regulates growth differentiation factor 15 mRNA stability in trophoblast.<sup>59</sup> Our data showed that KLB upregulation decreased the binding of FXR1 to the 3'UTR region of TRPV6 mRNA, enhancing the abundance and mRNA stability of TRPV6. Moreover, overexpression of FXR1 decreased the abundance and mRNA stability of TRPV6 in KLBOE cells, supporting that KLB positively regulated TRPV6 mRNA stability by competitively binding to FXR1.

Taken together, we provide fine evidence supporting that intestinal epithelial KLB is a critical protective factor in alcohol-induced intestinal barrier dysfunction and subsequent liver injury. As shown in Figure 7i, alcohol decreases intestinal KLB expression by inhibiting HNF4A, inducing the endocytosis and degradation of Occludin and ZO-1 protein and hence intestinal

epithelial hyperpermeability as well as ALD. When KLB was upregulated in the intestine, the binding of FXR1 to the 3'UTR region of TRPV6 was competitively decreased, promoting TRPV6 mRNA stabilization and its expression. Then KLB formed a complex with TRPV6, Occludin and ZO-1, preventing TJ proteins from degradation via endocytosis pathway, which facilitates the maintenance of intestinal epithelial integrity in the presence of alcohol (Figure 7i). Thus, our study suggests that dietary approaches and pharmacological agents that specifically activate intestinal KLB could be developed to prevent/treat ALD and other intestinal barrier dysfunction-associated diseases.

#### Contributors

L.Z., G.W. and X.R. designed the study and supervised the experimental work. Z.H., Q.D., Y.L., Z.Z., F.Y, Y.L., X.W. J.X. and W.C. performed all the experiments; L.Z., X.R., G.W., Z.H., Q.D. and Y.L. analyzed the data and wrote the manuscript. L.Z., Q.D. and Z.H. have verified the underlying data. All authors had access to the data and had reviewed the manuscript and approved the submitted version.

#### Data sharing statement

The datasets generated during the current study will be available from the corresponding author on reasonable request.

#### Declaration of interests

The authors declared there are no conflicts of interest.

#### Acknowledgement

The study was supported by grants from the National Natural Science Foundation of China (81970510, 81873571), Chongqing Natural Science Foundation (cstc2021ycjh-bgzxm0146, cstc2019jcyj-msxmX0336), Talent Project of Chongqing (CQYC201905079) and the Science and Technology Research Program of Chongqing Municipal Education Commission (KJQN2019000438).

#### Supplementary materials

Supplementary material associated with this article can be found in the online version at doi:10.1016/j.ebiom.2022.104181.

#### References

- 1 Singal AK, Mathurin P. Diagnosis and treatment of alcohol-associated liver disease: a review. *JAMA*. 2021;326(2):165–176.
- 2 Seitz HK, Bataller R, Cortez-Pinto H, et al. Alcoholic liver disease. *Nat Rev Dis Primers*. 2018;4(1):16.
- 3 Albillos A, de Gottardi A, Rescigno M. The gut-liver axis in liver disease: pathophysiological basis for therapy. *J Hepatol*. 2020;72(3):558–577.
- 4 Kayama H, Okumura R, Takeda K. Interaction between the microbiota, epithelia, and immune cells in the intestine. *Annu Rev Immunol*. 2020;38:23–48.

- 5 Yu L-X, Schwabe RF. The gut microbiome and liver cancer: mechanisms and clinical translation. *Nat Rev Gastroenterol Hepatol*. 2017;14(9):527–539.
- 6 Ferrere G, Wrzosek L, Cailleux F, et al. Fecal microbiota manipulation prevents dysbiosis and alcohol-induced liver injury in mice. *J Hepatol*. 2017;66(4):806–815.
- 7 Ito S, Kinoshita S, Shiraishi N, et al. Molecular cloning and expression analyses of mouse *betaklotho*, which encodes a novel *Klotho* family protein. *Mech Dev*. 2000;98(1-2):115–119.
- 8 Lan T, Morgan DA, Rahmouni K, et al. FGF19, FGF21, and an FGFRI/ $\beta$ -klotho-activating antibody act on the nervous system to regulate body weight and glycemia. *Cell Metab*. 2017;26(5):709–718.e3.
- 9 Benoit B, Meunier E, Castelli M, et al. Fibroblast growth factor 19 regulates skeletal muscle mass and ameliorates muscle wasting in mice. *Nat Med*. 2017;23(8):990–996.
- 10 Lin BC, Wang M, Blackmore C, Desnoyers LR. Liver-specific activities of FGF19 require *Klotho* beta. *J Biol Chem*. 2007;282(37):27277–27284.
- 11 Ji F, Liu Y, Hao J-G, et al. gene polymorphism is associated with obesity and non-alcoholic fatty liver disease in the Han Chinese. *Aging*. 2019;11(18):7847–7858.
- 12 Wong BS, Camilleri M, Carlson PJ, et al. A *Klotho* $\beta$  variant mediates protein stability and associates with colon transit in irritable bowel syndrome with diarrhea. *Gastroenterology*. 2011;140(7):1934–1942.
- 13 Dongiovanni P, Crudele A, Panera N, et al.  $\beta$ -*Klotho* gene variation is associated with liver damage in children with NAFLD. *J Hepatol*. 2020;72(3):411–419.
- 14 Panera N, Meroni M, Longo M, et al. The KLB rs17618244 gene variant is associated with fibrosing MAFLD by promoting hepatic stellate cell activation. *EBioMedicine*. 2021;65:103249.
- 15 Clarke TK, Adams MJ, Davies G, et al. Genome-wide association study of alcohol consumption and genetic overlap with other health-related traits in UK Biobank ( $N=112\ 117$ ). *Mol Psychiatry*. 2017;22(10):1376–1384.
- 16 Thompson A, Cook J, Choquet H, et al. Functional validity, role, and implications of heavy alcohol consumption genetic loci. *Sci Adv*. 2020;6(3):eaay5034.
- 17 Schumann G, Liu C, O'Reilly P, et al. KLB is associated with alcohol drinking, and its gene product  $\beta$ -*Klotho* is necessary for FGF21 regulation of alcohol preference. *Proc Natl Acad Sci USA*. 2016;113(50):14372–14377.
- 18 Garcia MA, Nelson WJ, Chavez N. Cell-cell junctions organize structural and signaling networks. *Cold Spring Harb Perspect Biol*. 2018;10(4):a029181.
- 19 Förster C. Tight junctions and the modulation of barrier function in disease. *Histochem Cell Biol*. 2008;130(1):55–70.
- 20 Mitic LL, Anderson JM. Molecular architecture of tight junctions. *Annu Rev Physiol*. 1998;60:121–142.
- 21 González-Mariscal L, Betanzos A, Nava P, Jaramillo BE. Tight junction proteins. *Prog Biophys Mol Biol*. 2003;81(1):1–44.
- 22 Cresci GA, Bush K, Nagy LE. Tributyrin supplementation protects mice from acute ethanol-induced gut injury. *Alcohol Clin Exp Res*. 2014;38(6):1489–1501.
- 23 Sang L, Kang K, Sun Y, Li Y, Chang B. FOXO4 ameliorates alcohol-induced chronic liver injury via inhibiting NF- $\kappa$ B and modulating gut microbiota in C57BL/6J mice. *Int Immunopharmacol*. 2021;96:107572.
- 24 Woudenberg-Vrenken TE, Lameris AL, et al. Functional TRPV6 channels are crucial for transepithelial  $Ca^{2+}$  absorption. *Am J Physiol Gastrointest Liver Physiol*. 2012;303(7):G879–G885.
- 25 Himmel NJ, Cox DN. Transient receptor potential channels: current perspectives on evolution, structure, function and nomenclature. *Proc Biol Sci*. 2020;287(1933):20201309.
- 26 Kärki T, Rajakylä EK, Acheva A, Tojkander S. TRPV6 calcium channel directs homeostasis of the mammary epithelial sheets and controls epithelial mesenchymal transition. *Sci Rep*. 2020;10(1):14683.
- 27 Cha S-K, Ortega B, Kurosu H, Rosenblatt KP, Kuro-O M, Huang C-L. Removal of sialic acid involving *Klotho* causes cell-surface retention of TRPV5 channel via binding to galectin-1. *Proc Natl Acad Sci USA*. 2008;105(28):9805–9810.
- 28 Chang Q, Hoefs S, van der Kemp AW, Topala CN, Bindels RJ, Hoenderop JG. The beta-glucuronidase *klotho* hydrolyzes and activates the TRPV5 channel. *Science*. 2005;310(5747):490–493.
- 29 Li D, Hu Z, He Q, et al. Lactoferrin alleviates acute alcoholic liver injury by improving redox-stress response capacity in female C57BL/6J mice. *J Agric Food Chem*. 2021;69(49):14856–14867.
- 30 Frezza M, di Padova C, Pozzato G, Terpin M, Baraona E, Lieber CS. High blood alcohol levels in women. The role of decreased gastric alcohol dehydrogenase activity and first-pass metabolism. *N Engl J Med*. 1990;322(2):95–99.
- 31 Shao T, Zhao C, Li F, et al. Intestinal HIF-1 $\alpha$  deletion exacerbates alcoholic liver disease by inducing intestinal dysbiosis and barrier dysfunction. *J Hepatol*. 2018;69(4):886–895.
- 32 Xu B, Jiang M, Chu Y, et al. Gasdermin D plays a key role as a pyroptosis executor of non-alcoholic steatohepatitis in humans and mice. *J Hepatol*. 2018;68(4):773–782.
- 33 Düring DN, Dittrich F, Rocha MD, et al. Fast retrograde access to projection neuron circuits underlying vocal learning in songbirds. *Cell Rep*. 2020;33(6):108364.
- 34 Heo MJ, Kim TH, You JS, Blaya D, Sancho-Bru P, Kim SG. Alcohol dysregulates miR-148a in hepatocytes through FoxO1, facilitating pyroptosis via TXNIP overexpression. *Gut*. 2019;68(4):708–720.
- 35 Ma TY, Nguyen D, Bui V, Nguyen H, Hoa N. Ethanol modulation of intestinal epithelial tight junction barrier. *Am J Physiol*. 1999;276(4):G965–G974.
- 36 Chen XY, Butt AM, Mohd Amin MCI. Enhanced paracellular delivery of vaccine by hydrogel microparticles-mediated reversible tight junction opening for effective oral immunization. *J Control Release*. 2019;311–312:50–64.
- 37 Kim S-Y, Yang D, Myeong J, et al. Regulation of calcium influx and signaling pathway in cancer cells via TRPV6-Numb1 interaction. *Cell Calcium*. 2013;53(2):102–111.
- 38 Tomilin VN, Cherezova AL, Negulyaev YA, Semenova SB. TRPV5/V6 channels mediate  $Ca^{2+}$  influx in jurkat T cells under the control of extracellular pH. *J Cell Biochem*. 2016;117(1):197–206.
- 39 Bajaj JS. Alcohol, liver disease and the gut microbiota. *Nat Rev Gastroenterol Hepatol*. 2019;16(4):235–246.
- 40 Garrison WD, Battle MA, Yang C, Kaestner KH, Sladek FM, Duncan SA. Hepatocyte nuclear factor 4alpha is essential for embryonic development of the mouse colon. *Gastroenterology*. 2006;130(4):1207–1220.
- 41 Ahn S-H, Shah YM, Inoue J, et al. Hepatocyte nuclear factor 4alpha in the intestinal epithelial cells protects against inflammatory bowel disease. *Inflamm Bowel Dis*. 2008;14(7):908–920.
- 42 Davison JM, Lickwar CR, Song L, Breton G, Crawford GE, Rawls JF. Microbiota regulate intestinal epithelial gene expression by suppressing the transcription factor Hepatocyte nuclear factor 4 alpha. *Genome Res*. 2017;27(7):1195–1206.
- 43 Kurosu H, Choi M, Ogawa Y, et al. Tissue-specific expression of beta*Klotho* and fibroblast growth factor (FGF) receptor isoforms determines metabolic activity of FGF19 and FGF21. *J Biol Chem*. 2007;282(37):26687–26695.
- 44 Wu G, Liu Y, Liu Y, et al. FGF 21 deficiency slows gastric emptying and reduces initial blood alcohol concentration in mice exposed to acute alcohol in fasting state. *Biochem Biophys Res Commun*. 2018;497(1):46–50.
- 45 Desai BN, Singhal G, Watanabe M, et al. Fibroblast growth factor 21 (FGF21) is robustly induced by ethanol and has a protective role in ethanol associated liver injury. *Mol Metabol*. 2017;6(11):1395–1406.
- 46 Liu Y, Zhao C, Xiao J, et al. Fibroblast growth factor 21 deficiency exacerbates chronic alcohol-induced hepatic steatosis and injury. *Sci Rep*. 2016;6:31026.
- 47 Antón M, Rodríguez-González A, Ballesta A, et al. Alcohol binge disrupts the rat intestinal barrier: the partial protective role of oleoylethanolamide. *Br J Pharmacol*. 2018;175(24):4464–4479.
- 48 Saitou M, Furuse M, Sasaki H, et al. Complex phenotype of mice lacking occludin, a component of tight junction strands. *Mol Biol Cell*. 2000;11(12):4131–4142.
- 49 O'Driscoll MC, Daly SB, Urquhart JE, et al. Recessive mutations in the gene encoding the tight junction protein occludin cause band-like calcification with simplified gyration and polymicrogyria. *Am J Hum Genet*. 2010;87(3):354–364.
- 50 McNeil E, Capaldo CT, Macara JG. Zonula occludens-1 function in the assembly of tight junctions in Madin-Darby canine kidney epithelial cells. *Mol Biol Cell*. 2006;17(4):1922–1932.
- 51 Phua DCY, Xu J, Ali SM, Boey A, Gounko NV, Hunziker W. ZO-1 and ZO-2 are required for extra-embryonic endoderm integrity, primitive ectoderm survival and normal cavitation in embryoid bodies derived from mouse embryonic stem cells. *PLoS One*. 2014;9(6):e99532.

- 52 Stamatovic SM, Johnson AM, Sladojevic N, Keep RF, Andjelkovic AV. Endocytosis of tight junction proteins and the regulation of degradation and recycling. *Ann N Y Acad Sci.* 2017;1397(1):54–65.
- 53 Marchiando AM, Shen L, Graham WV, et al. Caveolin-1-dependent occludin endocytosis is required for TNF-induced tight junction regulation in vivo. *J Cell Biol.* 2010;189(1):111–126.
- 54 Rincon-Heredia R, Flores-Benitez D, Flores-Maldonado C, et al. Ouabain induces endocytosis and degradation of tight junction proteins through ERK1/2-dependent pathways. *Exp Cell Res.* 2014;320(1):108–118.
- 55 Liviero F, Campisi M, Mason P, Pavanello S. Transient receptor potential vanilloid subtype 1: potential role in infection, susceptibility, symptoms and treatment of COVID-19. *Front Med (Lausanne).* 2021;8:753819.
- 56 Bobkov D, Yudintceva N, Lomert E, Shatrova A, Kever L, Semenova S. Lipid raft integrity is required for human leukemia Jurkat T-cell migratory activity. *Biochim Biophys Acta Mol Cell Biol Lipids.* 2021;1866(6):158917.
- 57 Majumder M, Johnson RH, Palanisamy V. Fragile X-related protein family: a double-edged sword in neurodevelopmental disorders and cancer. *Crit Rev Biochem Mol Biol.* 2020;55(5):409–424.
- 58 Cao H, Gao R, Yu C, Chen L, Feng Y. The RNA-binding protein FXR1 modulates prostate cancer progression by regulating FBXO4. *Funct Integr Genomics.* 2019;19(3):487–496.
- 59 Hong W, Chen JH, Ma HJ, Li L, Li XC. Fragile X-related protein 1 (FXR1) promotes trophoblast migration at early pregnancy via downregulation of GDF-15 expression. *Reprod Sci.* 2022;29(1):110–121.